PHYSICAL REVIEW B **95**, 140502(R) (2017)

Signatures of unconventional superconductivity in the $LaAlO_3/SrTiO_3$ two-dimensional system

D. Stornaiuolo,[1,2,*] D. Massarotti,[1,2] R. Di Capua,[1,2] P. Lucignano,[2] G. P. Pepe,[1,2] M. Salluzzo,[2] and F. Tafuri[3]
[1]*Dipartimento di Fisica "E. Pancini", Università di Napoli Federico II, Monte S. Angelo-Via Cintia, I-80126 Napoli, Italy*
[2]*CNR-SPIN UOS Napoli, Monte S. Angelo-Via Cintia, I-80126, Napoli, Italy*
[3]*Dipartimento di Ingegneria Industriale e dell'Informazione, Seconda Università di Napoli, I-81031 Aversa (CE), Italy*
(Received 19 January 2017; published 7 April 2017)

We study the superconducting state of the two-dimensional electron gas (2DEG) at the $LaAlO_3/SrTiO_3$ interface using Josephson junctions as spectroscopic probes. The transport properties of these devices reveal the presence of two superconducting gap structures and of an unconventional superconducting π channel. These features provide evidence of an unconventional superconducting ground state, possibly related to the interplay between superconductivity and the large Rashba spin-orbit coupling in the 2DEG.

DOI: 10.1103/PhysRevB.95.140502

I. INTRODUCTION

In the quest for exotic superconductivity, artificial superconductors have been pursued by coupling BCS s-wave superconductors and ferromagnetic materials, obtaining a triplet superconducting order parameter [1], while spinless p-wave superconductivity can be obtained in nanostructures hosting spin-orbit interactions, such as a semiconducting nanowire connected to superconducting electrodes [2]. The latter hybrid structures were used, for instance, to pursue excitations behaving as Majorana fermions [3]. In the two-dimensional electron gas (2DEG) at the $LaAlO_3/SrTiO_3$ (LAO/STO) interface, the combination of 2D superconductivity and Rashba spin-orbit coupling (SOC) is expected to give rise to an unconventional superconducting ground state [4,5], including a mix of spin-singlet and spin-triplet components [6,7]. The nature of superconductivity in LAO/STO and its interplay with SOC are, however, still largely unexplored. Scanning superconducting quantum interference device (SQUID) microscopy was used to evaluate the superfluid density as a function of the temperature, and the experimental results were interpreted using the standard BCS theory [8]. A recent work reports the observation of superconducting pairing in LAO/STO well above the superconducting critical temperature [9]. Moreover, tunneling spectroscopy along the interface normal direction in micrometer-sized Au-insulating (LAO)-superconducting (2DEG) junctions showed evidence of a gap with a BCS-like temperature dependence evolving into a pseudogap in the underdoped region of the phase diagram [10]. Here, we use nanoscale Josephson junctions (JJs) as an ultrasensitive spectroscopic tool to probe the superconducting gap and the order parameter symmetry of the 2DEG.

II. DEVICE DESIGN AND FABRICATION

We realized LAO/STO JJs using the Dayem bridge layout, where weak coupling between two superconducting banks is achieved through a constriction whose size is comparable to the superconducting coherence length ξ [11] (for LAO/STO $\xi \approx$ 50–70 nm [12]). A TiO_2 terminated STO single crystal was partially covered by an amorphous STO mask using e-beam lithography and a lift-off technique. Subsequently, a 10 unit cell (u.c.) LAO film was deposited using pulsed laser deposition, with a deposition temperature of 800 °C and 10^{-4} mbar of oxygen. Immediately after, the sample was annealed in oxygen. This technique has been previously employed to realize high-quality LAO/STO nanobridges and nanodevices [13,14]. Figure 1(a) shows a sketch of the geometry of our devices and Fig. 1(b) shows an atomic force microscope image of a typical JJ realized.

III. GENERAL PROPERTIES

The nanoscale JJs were measured down to dilution temperatures using low noise electronics (see Supplemental Material [15]) and their properties were tuned using electric field effect in the back gate configuration. Typical current versus voltage (I-V) characteristics are shown in Fig. 1(c). They refer to device 1, having $w = L = 200$ nm (with w and L being the nominal width and length of the constriction, respectively) and were recorded at $T = 50$ mK for different values of the gate voltage V_g, which tunes the magnitude of the critical current I_c, as well as the normal state resistance R_N. In these curves, the switching from the superconducting to the normal state is markedly rounded, as a consequence of thermal fluctuations, which are particularly relevant in low critical current JJs [16,17]. As shown in Fig. 1(d), the field effect tuned I_cR_N product increases up to 45 μV at $V_g = 11$ V, then shows a saturation, followed by a slight decrease, thus reflecting the the superconducting dome of LAO/STO. A similar behavior is found on different devices, as shown in the following.

IV. DIFFERENTIAL CONDUCTANCE AND MAGNETIC PATTERN MEASUREMENTS

Spectroscopic measurements on JJs can give direct access to the superconducting gap. With this aim, we performed differential conductance measurements as a function of the temperature and of the gate voltage. Figure 2 shows typical dI/dV vs V curves measured for two different devices. Figures 2(a) and 2(b) show measurements performed on device 1 keeping the gate voltage V_g fixed at 12 V and changing the temperature. Figure 2(c) shows measurements on device 2 performed keeping the temperature fixed at $T = 50$ mK and changing the gate voltage. We point out that device 2 has

*stornaiuolo@fisica.unina.it

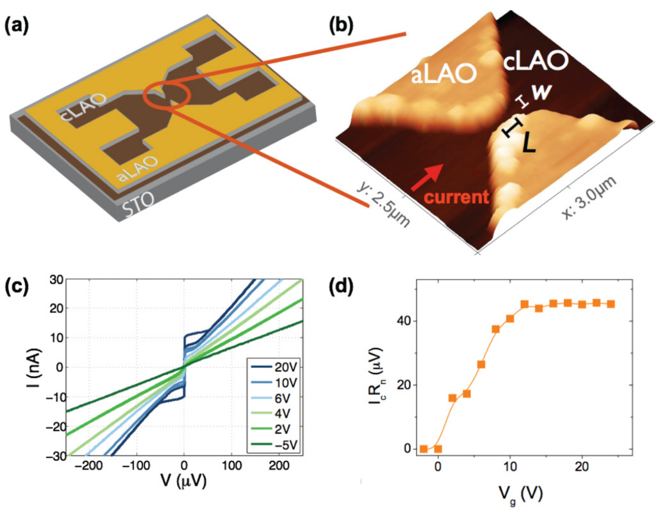

FIG. 1. Structure and general properties of LAO/STO JJs. (a) shows a sketch of the constriction layout used to realize the junctions. An atomic force microscope image of a typical constriction is shown in (b). W and L indicate the width and the length of the constriction, respectively, with the current flowing along the x axis. Typical I-V characteristics of a LAO/STO JJ ($w = L = 200$ nm) acquired at $T = 50$ mK are shown in (c). (d) shows I_cR_N vs V_g extracted from these measurements (using a $V = 5\ \mu$V criterion for the I_c).

a larger L/w ratio compared to that of device 1, hence it shows a different gate voltage response. All the data shown in Fig. 2 exhibit a double-peak structure, indicated by the arrows, evolving with the temperature and with V_g. Since we performed measurements on JJs with a slightly different geometry and using two different cryogenic and acquisition setups (see the Supplemental Material), we can confidently exclude geometrical and/or instrumental artifacts as the source of the observed behaviors.

The presence of two peaks in the conductance data indicates a two-gap superconducting state. We fit the conductance curves using a superconducting two-gap model [solid red lines in Figs. 2(b) and 2(c), discussed in detail in the Supplemental Material]. In Figs. 3(a) and 3(b) we show the results of the fits as a function of the temperature. The temperature behavior of the lowest-energy gap Δ_1 [Fig. 3(b)] is consistent with that of a BCS-like superconducting gap (solid red line) [11] having $\Delta_1(T = 0)/k_BT_1 = 1.7$ and $T_1 = 110$ mK. The second gap Δ_2 [Fig. 3(a)] shows a marked decrease around 90–100 mK but does not close at T_1. At the same time, the conductance curves measured for $T > T_1$ still show a clear peak at zero bias [Fig. 2(a)], associated with the persistence of a superconducting channel we attribute to Δ_2. The fit of the conductance curves using a two-superconducting-gap model is in good agreement with the temperature behavior of I_c extracted from the I-V curves, shown in Fig. 3(c). The $I_c(T)$ data can be reproduced assuming the presence of two superconducting channels with two different energy scales: one associated with Δ_1 with $T_1 = 110$ mK and a second one (contributing about 16% to the total critical current at 50 mK), associated with Δ_2 with $T_2 = 250$ mK (solid red line; more details on the fitting procedure and parameters can be found in the Supplemental Material).

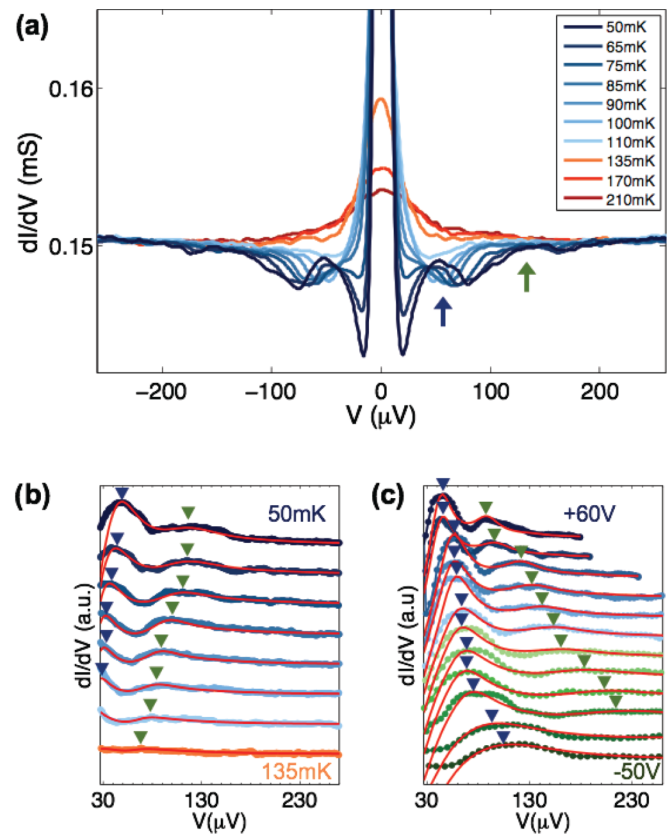

FIG. 2. Conductance dI/dV vs voltage V curves of LAO/STO JJs. The data in (a) were acquired for device 1 keeping fixed the gate voltage at $V_g = 12$ V and changing the temperature. The same data after subtraction of the background are reported in (b) (see Supplemental Material for details). (c) shows dI/dV vs V curves of device 2 acquired at $T = 50$ mK as a function of V_g, after subtraction of the background. Red lines in (b) and (c) are the fit of the conductance curves performed using a two-gap model. The data in (b) and (c) are plotted starting from $V = 26\ \mu$V as the fit cannot take into account the Josephson peak in the conductance.

Figures 3(d) and 3(e) show the values of Δ_2 and Δ_1 respectively as a function of the gate voltage extracted from the fit in Fig. 2(c) (referring to device 2 measured at $T = 50$ mK). Interestingly, both gap values increase with decreasing gate voltage, thus not following the phase diagram traced by the I_cR_N product in the underdoped region [i.e.. for $V_g < 0$ V, Fig. 3(f)]. The same behavior was found for the single gap reported in Ref. [10] (see Ref. [18]). In the optimally and slightly overdoped region, on the other hand, Δ_1 and Δ_2 scale in accordance with the I_cR_N product. In summary, the analysis of the conductance data and of the I_c vs T behavior indicates that both features are real superconducting gaps.

From the two-gap fit model, we can also extract the ratio between the partial density of states at the Fermi level, associated to the two gaps $\nu = N_2(0)/N_1(0) = \Gamma_{12}/\Gamma_{21}$ [19], where Γ_{12} and Γ_{21} are the interchannel scattering rates obtained from the conductance curve fits (Fig. 2). The inset of Fig. 3(d) shows that ν increases with the gate voltage; this means that the electric field effect increases the density of states N_2 more than N_1. We point out that the field effect tuned Rashba SOC in the 2DEG at the LAO/STO interface increases

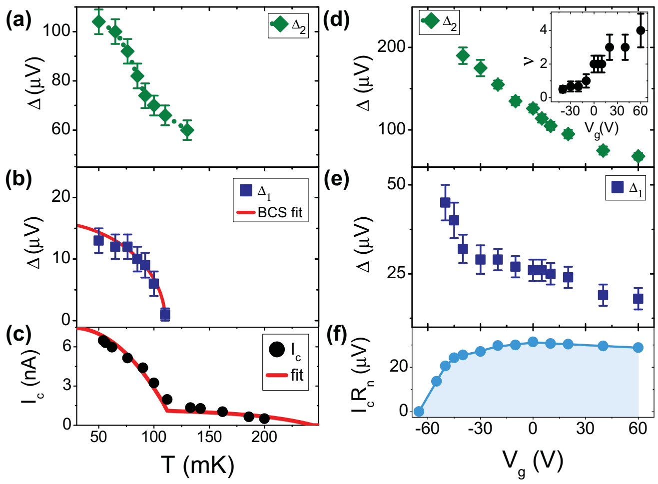

FIG. 3. Temperature and gate voltage behavior of the gap structures. (a) and (b) show the gap values as a function of the temperature as extracted from the fit of the dI/dV curves shown in Fig. 2(b) (device 1). The solid red line in (b) is the BCS fit of Δ_1 vs T. (c) shows the I_c vs T data, extracted using a $V = 5\ \mu$V criterion, from the I-V curves measured at $V_g = 9$ V. The solid red line is a fit performed using a two-gap model. (d) and (e) show the gap values as a function of V_g extracted from the fit of the dI/dV curves shown in Fig. 2(c) (device 2) and (f) shows the I_cR_N product for the corresponding V_g. In the inset of (d) we show the evolution of $\nu = N_2(0)/N_1(0)$ (with N_1 and N_2 the density of states at the Fermi level related to Δ_1 and Δ_2, respectively) as a function of the gate voltage V_g.

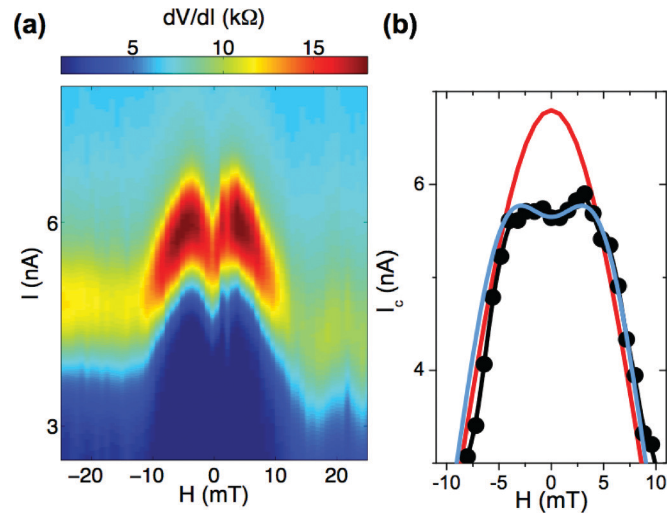

FIG. 4. Magnetic field behavior of LAO/STO junctions. (a) shows the differential resistance dV/dI, plotted as a function of the bias current and applied magnetic field, measured for device 1 at $T = 50$ mK and $V_g = 9$ V. (b) shows the extracted $I_c(H)$ pattern. A local minimum of the I_c at $H = 0$ is clearly visible. The solid red line is the classical Fraunhofer pattern whereas the blue line is the fit performed assuming the combination of a 0 and a π channel (see Supplemental Material for details).

as well with the increase of the carrier density. This similar behavior could indicate a link between the Rashba SOC and Δ_2.

The two superconducting gaps observed could be associated with the different electronic bands contributing to the transport of LAO/STO, in analogy with the interpretation of two-gap superconductivity reported in the tunneling studies of doped bulk STO [20]. However, there are several important differences between the electronic properties of bulk STO and those of LAO/STO 2DEG. Firstly, superconductivity in doped STO has been found for three-dimensional (3D) carrier concentrations spanning more than two orders of magnitude, from 1×10^{18} cm^{-3} to 4×10^{20} cm^{-3} [21], whereas superconductivity in LAO/STO 2DEG appears only for carrier concentrations above 10^{19} cm^{-3} (taking into account 2D-to-3D carrier concentration conversion) and is restricted to a much smaller range of carrier concentrations [22]. Secondly, the LAO/STO 2DEG is characterized by an inversion of the Ti $3d$-t_{2g} orbital bands compared to bulk STO, with the bottom of the d_{xy} band lying 50 meV below the $d_{xz/yz}$ ones [23,24]. Moreover, in LAO/STO, the large Rashba SOC energy, exceeding the characteristic superconducting scale of the system (T_c), should have a deep influence on the superconducting properties of the 2DEG. In particular, the presence of a multicomponent order parameter arising from the interplay between superconductivity and Rashba SOC is predicted [25]. We notice that the $I_c(T)$ data shown in Fig. 3(c) bear a close resemblance to those measured for heavy-fermion superconductor-based Josephson junctions [26]. In that work, the peculiar behavior of I_c was related to the presence of a complex order parameter.

In order to obtain further insight in the superconducting pairing state, we measured the magnetic patterns of the junctions. In Fig. 4(a) we show the differential resistance dV/dI in a color scale as a function of current bias and applied magnetic field measured for device 1 at $V_g = 9$ V and $T = 50$ mK. A general discussion on the magnetic behavior of the devices is reported in the Supplemental Material; here, we focus on the low field region where a local minimum of the dV/dI (hence, of the I_c) at $H = 0$ can be clearly distinguished. This feature was observed for different values of V_g; in all cases, the magnetic patterns are symmetric with respect to zero field and show no hysteresis upon reversal of the magnetic field sweep direction (see Supplemental Material). This excludes that the zero field minimum of I_c can be ascribed to the presence of a ferromagnetic (FM) barrier, in agreement with the absence of FM order demonstrated by x-ray magnetic circular dichroism on LAO/STO samples grown in the same conditions [27]. A zero field minimum of the I_c can be, on the other hand, explained with the interference, inside the junction, between channels characterized by order parameters with different internal phase shifts [28], namely, a 0 and a π channel. A fit of the $I_c(H)$ pattern assuming such a combination is shown as a solid blue line in Fig. 4(b) and is in excellent agreement with the experimental data. The depth of the zero field dip suggests a contribution of the π part of about 10% of the total supercurrent. It is worth noting that the two-channel fit of the I_c vs T behavior shown in Fig. 3(c) leads to a similar estimation for the unconventional channel contribution to the total I_c. The formation of a π channel in our LAO/STO JJs can be explained assuming an unconventional order parameter [29], in agreement with the prediction of a Rashba

SOC-induced multicomponent order parameter, where a singlet and a triplet component, of the p-wave type, are mixed. Supercurrent sign reversal, hence a π shift, is expected in a junction between p-wave superconductors in the presence of time reversal symmetry (TRS) breaking mechanisms [30]. In our case, TRS could be either spontaneous [31] or due to local inhomogeneity of the superconducting order parameter [32], as induced, for instance, by the predicted intrinsic segregation of high SOC regions at the LAO/STO interface [33]. Another scenario involves the existence of protected transport channels as recently inferred from transport measurements in LAO/STO [34,35] and proposed by theoretical calculations [36,37].

V. CONCLUSIONS

In conclusion, our study of LAO/STO JJs gives evidence of unconventional superconductivity in this system. The conductance spectra and the I_c vs T behavior indicate the presence of two superconducting gap structures, and the I_c vs H patterns show anomalies that can be accounted for only by assuming the presence of an unconventional order parameter. Although more experimental work is needed in order to firmly establish the details of the superconducting state of LAO/STO, we point out that our results are in agreement with theoretical predictions of mixed singlet-triplet superconducting order parameters in 2D systems hosting Rashba SOC and pave the way to a deeper understanding of these systems. The ability to create and study elusive unconventional superconducting states is a confirmation of the fascinating possibilities offered by engineered oxides for the study of exotic excitations and the realization of novel quantum electronics [38].

ACKNOWLEDGMENTS

The authors thank J.-M. Triscone and S. Gariglio for their continuous support to this research. We thank M. Sigrist for comments that greatly improved the manuscript, A. D. Caviglia and M. Gabay for useful discussions, B. Jouault for help with data treatment, A. F. Morpurgo for giving us the possibility to use his electron beam lithography and dilution facilities, and F. Lombardi for preliminary measurements. This work was partly supported by the Italian MIUR FIRB project HybridNanoDev RBFR1236VV.

[1] F. Bergeret, A. Volkov, and K. Efetov, Rev. Mod. Phys. **77**, 1321 (2005).
[2] J. Alicea, Rep. Prog. Phys. **75**, 076501 (2012).
[3] D. Bercioux and P. Lucignano, Rep. Prog. Phys. **78**, 106001 (2015).
[4] K. Yada, S. Onari, Y. Tanaka, and J.-i. Inoue, Phys. Rev. B **80**, 140509 (2009).
[5] M. S. Scheurer and J. Schmalian, Nat. Commun. **6**, 6005 (2015).
[6] V. Kozii and L. Fu, Phys. Rev. Lett. **115**, 207002 (2015).
[7] S. Nakosai, Y. Tanaka, and N. Nagaosa, Phys. Rev. Lett. **108**, 147003 (2012).
[8] J. A. Bert, K. C. Nowack, B. Kalisky, H. Noad, J. R. Kirtley, C. Bell, H. K. Sato, M. Hosoda, Y. Hikita, H. Y. Hwang *et al.*, Phys. Rev. B **86**, 060503 (2012).
[9] G. Cheng, M. Tomczyk, S. Lu, J. P. Veazey, M. Huang, P. Irvin, S. Ryu, H. Lee, C.-B. Eom, C. S. Hellberg *et al.*, Nature (London) **521**, 196 (2015).
[10] C. Richter, H. Boschker, W. Dietsche, E. Fillis-Tsirakis, R. Jany, F. Loder, L. Kourkoutis, D. Muller, J. Kirtley, C. Schneider *et al.*, Nature (London) **502**, 528 (2013).
[11] M. Tinkham, *Introduction to Superconductivity* (Courier Corporation, 1996).
[12] A. Caviglia, S. Gariglio, N. Reyren, D. Jaccard, T. Schneider, M. Gabay, S. Thiel, G. Hammerl, J. Mannhart, and J.-M. Triscone, Nature (London) **456**, 624 (2008).
[13] D. Stornaiuolo, S. Gariglio, N. Couto, A. Fete, A. Caviglia, G. Seyfarth, D. Jaccard, A. Morpurgo, and J.-M. Triscone, Appl. Phys. Lett. **101**, 222601 (2012).
[14] D. Stornaiuolo, S. Gariglio, A. Fête, M. Gabay, D. Li, D. Massarotti, and J.-M. Triscone, Phys. Rev. B **90**, 235426 (2014).
[15] See Supplemental Material at http://link.aps.org/supplemental/10.1103/PhysRevB.95.140502 for details on the measurement technique and on the fit of the experimental data.
[16] J. M. Martinis and R. L. Kautz, Phys. Rev. Lett. **63**, 1507 (1989).
[17] D. Stornaiuolo, G. Rotoli, D. Massarotti, F. Carillo, L. Longobardi, F. Beltram, and F. Tafuri, Phys. Rev. B **87**, 134517 (2013).
[18] We observe that the values of the single gap reported in Ref. [10] are halfway between Δ_1 and Δ_2. This difference could be ascribed to the different geometry of the two experiments (vertical tunneling using large scale devices versus lateral transport of nanoscale junctions) leading to different tunneling matrix elements.
[19] N. Schopohl and K. Scharnberg, Solid State Commun. **22**, 371 (1977).
[20] G. Binnig, A. Baratoff, H. E. Hoenig, and J. G. Bednorz, Phys. Rev. Lett. **45**, 1352 (1980).
[21] X. Lin, G. Bridoux, A. Gourgout, G. Seyfarth, S. Krämer, M. Nardone, B. Fauqué, and K. Behnia, Phys. Rev. Lett. **112**, 207002 (2014).
[22] S. Gariglio, M. Gabay, and J.-M. Triscone, APL Mater. **4**, 060701 (2016).
[23] M. Salluzzo, J. Cezar, N. Brookes, V. Bisogni, G. De Luca, C. Richter, S. Thiel, J. Mannhart, M. Huijben, A. Brinkman *et al.*, Phys. Rev. Lett. **102**, 166804 (2009).
[24] P. Delugas, A. Filippetti, V. Fiorentini, D. I. Bilc, D. Fontaine, and P. Ghosez, Phys. Rev. Lett. **106**, 166807 (2011).
[25] L. P. Gor'kov and E. I. Rashba, Phys. Rev. Lett. **87**, 037004 (2001).
[26] J. Strand, D. Bahr, D. Van Harlingen, J. Davis, W. Gannon, and W. Halperin, Science **328**, 1368 (2010).
[27] M. Salluzzo, S. Gariglio, D. Stornaiuolo, V. Sessi, S. Rusponi, C. Piamonteze, G. De Luca, M. Minola, D. Marré, A. Gadaleta *et al.*, Phys. Rev. Lett. **111**, 087204 (2013).
[28] H. Sickinger, A. Lipman, M. Weides, R. G. Mints, H. Kohlstedt, D. Koelle, R. Kleiner, and E. Goldobin, Phys. Rev. Lett. **109**, 107002 (2012).
[29] 0-π junctions have been realized with conventional s-wave superconductors introducing a FM barrier. In these JJs, modulating

the thickness of the FM layer determines a change in the sign of the critical current, therefore in the phase of the junctions ground state (0 or π) [39]. The persistence of the unconventional behavior as a function of the gate voltage seen in our devices is in sharp contrast with this scenario.

[30] Y. Sawa, T. Yokoyama, Y. Tanaka, and A. A. Golubov, Phys. Rev. B **75**, 134508 (2007).
[31] P. M. R. Brydon, C. Iniotakis, D. Manske, and M. Sigrist, Phys. Rev. Lett. **104**, 197001 (2010).
[32] M. Sigrist, Prog. Theor. Phys. **99**, 899 (1998).
[33] N. Scopigno, D. Bucheli, S. Caprara, J. Biscaras, N. Bergeal, J. Lesueur, and M. Grilli, Phys. Rev. Lett. **116**, 026804 (2016).
[34] A. Fête, S. Gariglio, A. D. Caviglia, J.-M. Triscone, and M. Gabay, Phys. Rev. B **86**, 201105 (2012).
[35] G. Cheng, J. P. Veazey, P. Irvin, C. Cen, D. F. Bogorin, F. Bi, M. Huang, S. Lu, C.-W. Bark, S. Ryu *et al.*, Phys. Rev. X **3**, 011021 (2013).
[36] Y. Tanaka, T. Yokoyama, A. V. Balatsky, and N. Nagaosa, Phys. Rev. B **79**, 060505 (2009).
[37] Y. Asano and S. Yamano, Phys. Rev. B **84**, 064526 (2011).
[38] D. Stornaiuolo, C. Cantoni, G. M. De Luca, R. Di Capua, E. Di. Gennaro, G. Ghiringhelli, B. Jouault, D. Marre, D. Massarotti, F. Miletto Granozio *et al.*, Nat. Mater. **15**, 278 (2016).
[39] M. Weides, M. Kemmler, H. Kohlstedt, R. Waser, D. Koelle, R. Kleiner, and E. Goldobin, Phys. Rev. Lett. **97**, 247001 (2006).